Development of a mixed mode double cantilever beam specimen for the fracture characterization of adhesives under high displacement rate

Noëlig Dagorn, Gérald Portemont, Julien Berthe, François Rasselet, Benjamin Bourel, Franck Lauro

Development of a mixed mode double cantilever beam test for the fracture characterization of adhesives under dynamic loadings

Noëlig Dagorn[a,*], Gérald Portemont[c], Julien Berthe[c], François Rasselet[b], Benjamin Bourel[d], Franck Lauro[d]

[a] *Safran Composites, 33 avenue de la gare, Itteville 91760, France*
[b] *Département Mécanique des Matériaux et Composites, Safran Aircraft Engines, Rond-point René Ravaud - Réau, 77515 Moissy-Cramayel, France*
[c] *DMAS, ONERA, F-59014 Lille, France*
[d] *Laboratoire d'Automatique, de Mécanique et d'Informatique Industrielles et Humaines, Université Polytechnique Hauts de France, Valenciennes, France*

Abstract

In this paper, a new specimen called MMDCB is developed for the mixed mode fracture characterization of adhesives under dynamic loadings. The MMDCB specimen is designed using finite elements simulations in order to characterize a single mode mixity. Firstly, the MMDCB test is experimentally validated under quasi-static loading, compared to a reference Single Leg Bending test. The test results, obtained with the two different specimens, exhibit consistent evaluations of the mixed mode fracture toughness. Secondly, the MMDCB test under asymmetric dynamic loading is validated through explicit simulations. The Corrected Beam Theory with Effective crack length is numerically proved to accurately determine the mixed mode fracture toughness under a dynamic loading rate up to 1m/s.

Keywords: Adhesive joint, Dynamic loading, Mixed mode, Fracture toughness, Beam theory

∗. Corresponding Author
Email address: noelig.dagorn@safrangroup.com (Noëlig Dagorn)

Nomenclature

β	Angle of a bevel on the substrate section
δ	Displacement
$\dot{\delta}$	Displacement rate
$\pi/2 - \alpha$	Angle between the plane of the joint and the loading axis
ρ	Material density
σ_{II}	Mode II stress along the crack front
a	Crack length measurement using the Corrected Beam Theory with Effective crack length
a_0	Initial crack length in the single leg bending test
G	Energy release rate
G_t	Total energy release rate
G_{Ic}	Mode I critical energy release rate
G_{IIc}	Mode II critical energy release rate
G_{IIIc}	Mode III critical energy release rate
G_s	Shear energy release rate $G_{II} + G_{III}$
$P_{x/y}^{down}$	Vertical or Horizontal (x/y) Load at the lower part of the apparatus.
$P_{x/y}^{up}$	Vertical or Horizontal (x/y) Load at the upper part of the apparatus.
$z_{1/2}$	Respective vertical distance to the neutral fibre.
B	Length along the curvilinear abcissa of the crack front
E	Young Modulus of the substrates
I	Second moment of area of a substrate
M	Moment
P	Load

1. Introduction

Bonded joints present several advantages compared to riveting or welding techniques. Thus, adhesively bonded assemblies are widely developed in the automotive and aeronautic industries. In these fields of applications, the adhesives can be subject to high-velocity impact loadings. Therefore, failure can occur in the adhesive layer with a crack propagation. In such a case, the critical energy release rate G_c is a necessary parameter to predict the crack growth and the energy dissipated. In addition to this, under an impact event, the adhesive is

loaded under a whole range of both loading rates and loading states. For every crack tip, the loading state can be defined with a mode mixity between the three elementary fracture modes. These three fracture modes are the tensile opening Mode I, the in-plane shear Mode II and the anti-plane shear Mode III. It is well established that the fracture behaviour of adhesives depends both on the loading rate [1][2][3] and on the mode mixity [4][5]. The characterization of the adhesive failure under a controlled mode mixity is a challenging issue itself. Many fixtures were developed for this purpose [6][7] [8]. A well-known device for the mixed mode fracture characterization of composites is the Mixed Mode Bending (MMB) apparatus [9]. This complex apparatus was recently adapted to the characterization of bonded assemblies with metallic substrates [5][10]. In such a case, steel substrates with a high yield stress were necessary to avoid any plastic strain. The use of thick metallic substrates with a low yield stress was made possible with a similar, but even more sophisticated fixture [11]. These complex fixtures involve multiple contact points with a massive lever. Therefore, their inertia limits their application to quasi-static loading rates. On the other hand, recent studies report the mixed mode fracture rate-sensitivity of bonded composite joints with a simplified three point bending apparatus [12] [13]. However, under dynamic loading, delamination occurred in the composite substrates, instead of a failure in the joint. To the authors' knowledge, there is currently no suitable fixture for characterizing the mixed-mode dynamic fracture behaviour of adhesive joints with metallic substrates.

Thus, the authors present a new specimen named MMDCB, for the mixed mode fracture characterization of bonded joints, with metallic substrates, under dynamic loading rates. In the first section, the specimen design is carried out, considering aluminum substrates with a relatively low yield stress compared to steel. The second section presents an experimental investigation, performed on a viscoelastic viscoplastic epoxy adhesive, under quasi-static loading, in order to validate the new MMDCB specimen. The validation is made by comparison of the evaluated fracture toughness, with a reference single Leg Bending test. In the final section, numerical explicit computations are performed in order to discuss the use of MMDCB specimens with unsymmetric loading devices, such as servohydraulic machines.

2. MMDCB specimen

2.1. Specimen design

According to the literature, the Mode II and Mode III fracture toughnesses were experimentally found to be equal for epoxy adhesives [14]. Therefore, Mode II and Mode III will be assumed to be equivalent, and referred to as shear loading. In this section, the objective is to design an experimental setup that will allow the failure behavior of adhesives to be studied, with a constant mode mixity $G_s/G_t = \frac{G_{II}+G_{III}}{G_t}$, under dynamic loading rates. One way to control the mode mixity is to enforce an angle between the plane of the joint and the

loading axis. For instance, the ARCAN set-up [15], presented in Figure 1, allows several angles, and consequently, mode mixities to be chosen. It has been exten-

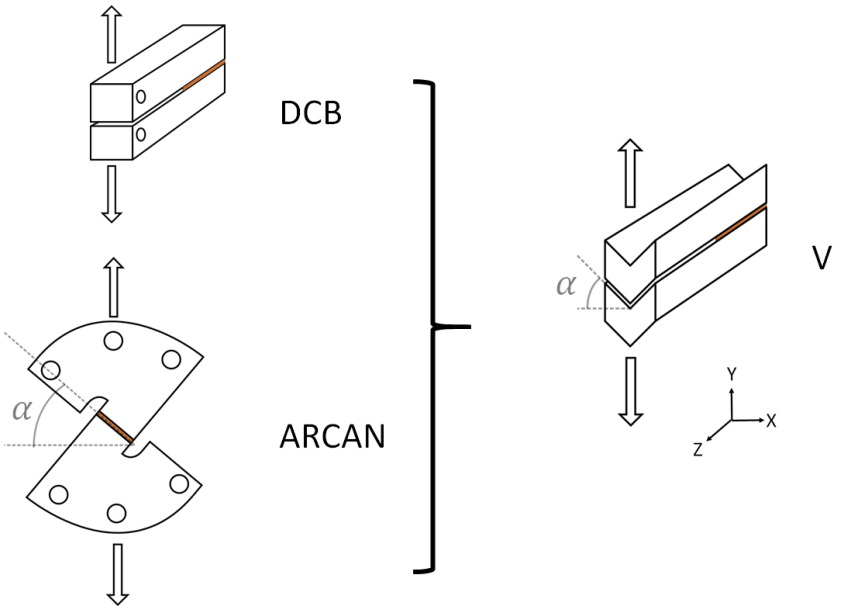

FIGURE 1: Schematic view of the combination between the DCB and the ARCAN tests into a V-shaped specimen with an inclined adhesive. Arrows represent the loading axis.

ded for the characterization of adhesives under both mixed mode and dynamic loading [3][16]. It was also adapted for the quasi-static fracture characterization of adhesives [17]. However, any small crack advance alters the global loading axis. Consequently, the mode mixity varied with the crack length. Thus, the fracture toughness evaluation was highly sensitive to the crack length measurement. In order to increase the confidence in the obtained value, the mode mixity should be independent from the crack length. The most common test that fulfils this condition is the DCB test [18], which is also presented in Figure 1. Whatever the crack position, the loading axis remains unchanged. This important property is guaranteed by two conditions. The first one is to ensure that the specimen respects a plane symmetry, defined by the crack propagation direction, and the loading axis. In Figure 1, this YZ plane symmetry avoids any torsion in the DCB substrates. The second condition is that the substrates must exhibit the same flexure. To do so, the substrates must share the same second moment of area, and consequently, the same section. In Figure 1, a "V"-shaped specimen inspired by the DCB and the ARCAN test is presented. This V-shaped specimen fulfils the two previously mentioned conditions and should maintain the advantage of the ARCAN test. The mode mixity is controlled by the angle α and is independent from the crack length.

However, a variation of the mode mixity remains along the crack front in this specimen. The V-shaped specimen section is presented in Figure 2a. There is a longitudinal Mode II stress gradient along the crack front. It can be expressed using the simple beam theory :

$$\sigma_{II} = \frac{M(z_2 - z_1)}{I} \tag{1}$$

Where M is the applied moment, I is the second moment of area of one arm, and z_1 and z_2 are the respective vertical distances to the neutral fibre. These two distances vary across the section of the V-shaped specimen.

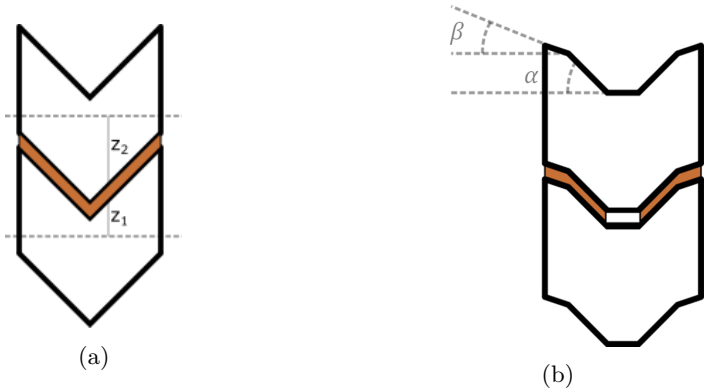

(a) (b)

FIGURE 2: (*a*) Transverse section of the V specimen : Dashed gray lines are the respective neutral fibres of each substrate. (*b*) Transverse section of the MMDCB specimen with $|\beta - \alpha| = 15°$

From Irwin's [19][20] theory and Equation (1), the Mode II energy release rate should be a quadratic function of the Mode II stress along the crack front. Thus, whatever the angle $\alpha > 0°$, the V-shaped specimen is expected to exhibit a quadratic Mode II variation along the crack front.

As a reminder, the aim is to determine the fracture toughness for a single mode mixity, which does not vary across the crack front. According to Equation (1), the absolute distance $|z_2 - z_1|$ should be restricted to lower the Mode II variations. The authors suggest a new geometry, whose section is detailed in Figure 2b. This new geometry will be to referred as Mixed Mode Double Cantilever Beam (MMDCB). Near the edge of the MMDCB section, a second angle β is formed to lower the shear stress contribution. The not bonded center part of the MMDCB specimen also avoids high values of $|z_2 - z_1|$. Moreover, according to equation (1), the Mode II contribution can be lowered using substrates with a high second moment of area. For the same nominal width and thickness, a MMDCB substrate has a higher second moment of area than a V-shaped one. Thus, the MMDCB specimen is expected to exhibit a more homogeneous mode mixity along the crack front.

2.2. Mode Mixity calculation

According to the Saint Venant principle, Equation (1) is valid far from the crack front. Thus, the mode mixity along the crack front should be more precisely evaluated. In order to compare the MMDCB and the V-shaped specimens, finite elements simulations are performed using the commercial code Abaqus 6.14. A 3D implicit model of the V-shaped specimen is presented in Figure 3a. Applying a YZ plane symmetry, only half of the specimen was modelled to minimize the simulation time. For visualization purposes, a YZ plane mirror was then applied, in order to observe the whole V-shaped specimen in Figure 3a. Two identical moments were applied on the respective surfaces of the V-shaped specimen. The mode mixity determination does not depend on the material parameters considered in the simulation. Thus, the authors arbitrarily chose to present simulations with materials used in the experimental work that follows. Aluminum substrates (E=73.1GPa, $\nu = 0.33$) were considered, using 1mm linear elastic wedge elements (C3D6). The element size was refined as 5% of the substrate thickness, less than the 10% ratio prescribed for mesh convergence in the DCB modelling with cohesive elements [21]. The adhesive was modelled with 200μm thick cohesive elements (COH8D4). These cohesive elements follow the substrates motion according to a tie constraint. A bi-linear cohesive law was considered with a quadratic nominal stress initiation criterion and a power law. The longitudinal stress field in the V-shaped section at the crack front is plotted in Figure 3b. The Mode II stress gradient near the crack tip is observable, and clearly in agreement with Equation (1).

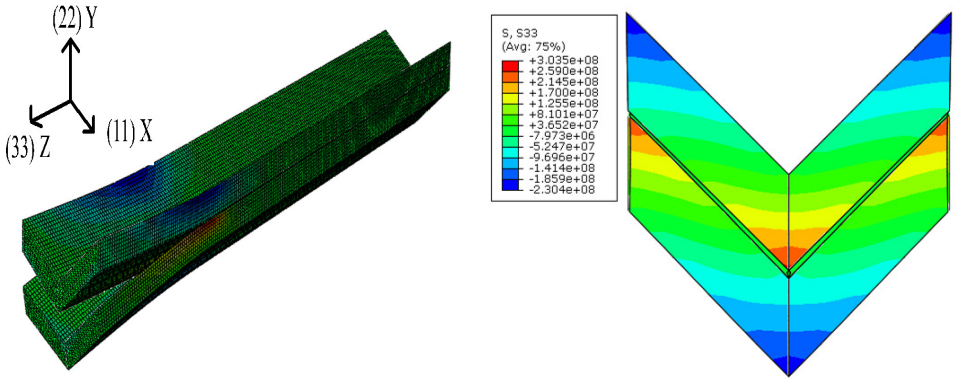

(a) (b)

FIGURE 3: (*a*) Longitudinal stress field σ_{zz}(Pa) in the "V"-shaped specimen ($\alpha = 45°$). (*b*) XY Cut view at the crack tip showing the Mode II distribution.

The mode mixity G_s/G_t is defined as the proportion of shear energy release rate with respect to the total energy release rate. It can be evaluated using the Abaqus output variable MMIXDME. To ensure that the mode mixity calculation is independent from the cohesive law, only values along the crack front are considered. The crack front is defined when the scalar damage variable D is

equal to 1. For an angle $\alpha = 45°$, the mode mixity G_s/G_t distribution across the section is plotted in Figure 4. A significant variation along the crack front is observed, with a standard deviation of 27%. The Mode II contribution can be easily evaluated through the mode mixity evolution along the crack front.

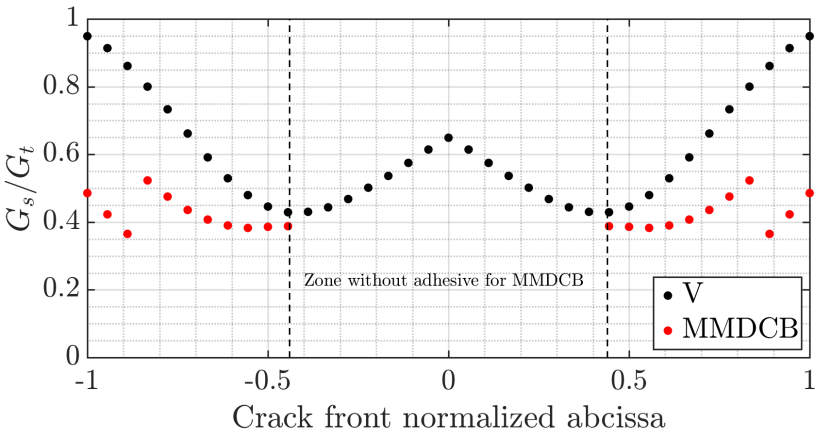

FIGURE 4: Mode mixity evolution along the crack front for the V geometry (black dots) and the MMDCB geometry (red dots). $\alpha = 45°$

In comparison, the mode mixity evolution for a MMDCB specimen with a small bevel $|\beta - \alpha = 15|°$ is also plotted. As the authors suggested in the previous section, a small bevel can lower the Mode III contribution. In addition, the higher second moment of area of the MMDCB substrates also lower the Mode II gradient compared to the V-shaped specimen. With a relatively small Mode II contribution, one can say that the MMDCB specimen is mainly loaded under Mode I and III. For $\alpha = 45°$, a mean mode mixity of $G_s/G_t = 42\%$ is obtained with a standard deviation of 11%. Thus, the MMDCB specimen provides a more homogeneous mode mixity distribution along the crack front than the V-shaped specimen.

α (°)	30	45	60
$< G_s/G_t >$ (%)	17.2	42.4	72.2
$\frac{\sigma}{<G_s/G_t>}$ (%)	16.4	11.7	8.9

TABLE 1: MMDCB mean value and standard deviation of the mode mixity along the crack front for different angles α

Table 1 summarizes the mode mixity that can be achieved by varying the main angle α. The full fracture envelope can be explored using MMDCB specimens, with a bevel $|\beta - \alpha| = 15°$, and with a varying angle α. Nevertheless, the mode mixity determination on the MMDCB geometry is based upon two statements.
Firstly, the MMDCB test is considered with two balanced crack fronts. Indeed,

the MMDCB specimen involves two bonded areas, and consequently two cracks which are balanced in the simulations. This assumption must be experimentally verified to ensure a constant mode mixity across the MMDCB section. The second statement is to consider Mode II and Mode III as equivalent according to the references for epoxy adhesives [14]. In order to validate this assumption, the MMDCB test should be compared to a reference test.

3. Quasi-static experimental validation

Only the MMDCB specimen with $\alpha = 45°$ is considered in what follows. This MMDCB specimen should provide a characterization of adhesives with $G_s/G_t = 42$ %. Consequently, it can be compared to the Single Leg Bending (SLB) test, which also provides a mode mixity $G_{II}/G_t = 42$ %. Therefore, the aim of this section is to compare the fracture toughness determination with these two tests. The MMDCB test is mainly loaded under Mode I and III, whereas the SLB test is loaded under Mode I and II. If the two G_c evaluations are found to be equal, it will confirm the assumption on the equivalence between the Mode II and the Mode III for epoxy adhesives.

3.1. Materials

For all specimens, 20 mm thick aluminum 2024T351 substrates were used. The surfaces were first machined to ensure a planeity of less than 50μm over the total bonding length. The substrates' surfaces were then treated using a phosphorus anodic oxidation bath. An epoxy primer provided by Solvay was applied on the bonding surfaces to improve adhesion. A viscoelastic viscoplastic epoxy adhesive provided by Safran Aircraft Engines was used. Following the supplier instructions, the specimens were cured for 360 minutes at 150 °C and at a pressure of 350 kPa. 40 μm thick non-adherend Teflon inserts were used. Thus, the crack directly initiates from the tip of the teflon film.

3.2. Single Leg Bending testing

The SLB test [22] is a mixed mode fracture test. The experimental setup is presented in Figure 5. The specimen is loaded with a three point bending apparatus. The bottom substrate remains free. The top one is subjected to flexure. The initial distance from the Teflon tip to the right contact point was taken as a_0=65 mm. Six 20 mm large SLB specimens were tested using an electromechanical testing machine (Instron 5887). The specimens were loaded at a crosshead speed of 0.5 mm/min. The displacement was measured under the lower substrate, at the centre of the specimen, with a Keyence laser displacement sensor. The central applied load was recorded with an Instron 2525-114 load cell, using a measurement range of 30 kN. For all specimens tested, an unstable crack propagation behaviour was observed with a significant drop in the load time history. The fracture surfaces observation suggests an initiation at the tip of the Teflon insert, in the adhesive layer. The crack then kinked at the interface

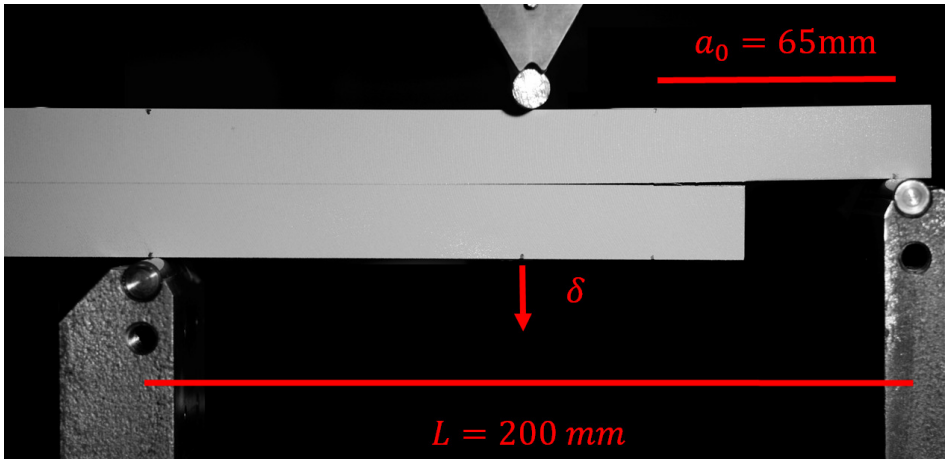

FIGURE 5: Photograph (after testing) of the SLB specimen. a_0 is the distance from the Teflon tip to the right contact point. δ is the displacement measured with the laser sensor.

between the epoxy adhesive and the substrate. Consequently, only the crack initiation in the epoxy joint is considered in the analysis.

In order to evaluate the fracture toughness, the authors chose to extend an analysis protocol, first proposed by Stamoulis et al. [5]. In their work, a 2D implicit simulation of the Mixed Mode Bending test was performed. The critical load to failure was used to calculate the Rice [23] J-integral at the crack tip of a joint. In this work, this approach was adapted to the SLB test. The SLB test was modelled using the commercial code Abaqus. An overview of the model is presented in Figure 6a. The boundary conditions at the three elastic steel rollers (E=210 GPa, ν=0.3) were controlled with respective reference points. Each roller was coupled to a reference point with a coupling constraint. The coupling was considered with a continuum distribution on the rollers. The two bottom rollers were built-in while the top one was loaded under a controlled vertical displacement. A surface-to-surface normal penalty contact interaction between each roller and the specimen was created. The interaction friction coefficient was taken as 0.3. The aluminum substrates and the rollers were modelled using plain strain CPE4R elements. Almost all of the elastic adhesive part was modelled with CPE3 elements. Indeed, a contour zone with a specific mesh is necessary to calculate the J-integral at the crack tip, as detailed in the work by Stamoulis et al. [5]. The mesh near the crack tip is plotted in Figure 6b.

The experimental and simulated Load-Displacement curves are plotted in Figure 7. The initial crack length was adjusted to a_0=73.5 mm in the simulation, in order to accurately model the specimen stiffness. The J-integral is determined from the experimentally obtained load to failure. Over the six tested specimens, the mean fracture toughness was found to be $G_c/G_{Ic} = 2.07$ with a standard deviation of 9.5 %. With a mode mixity of 42 %, it represents twice the Mode I fracture toughness G_{Ic} previously evaluated by the authors [24]. The mixed

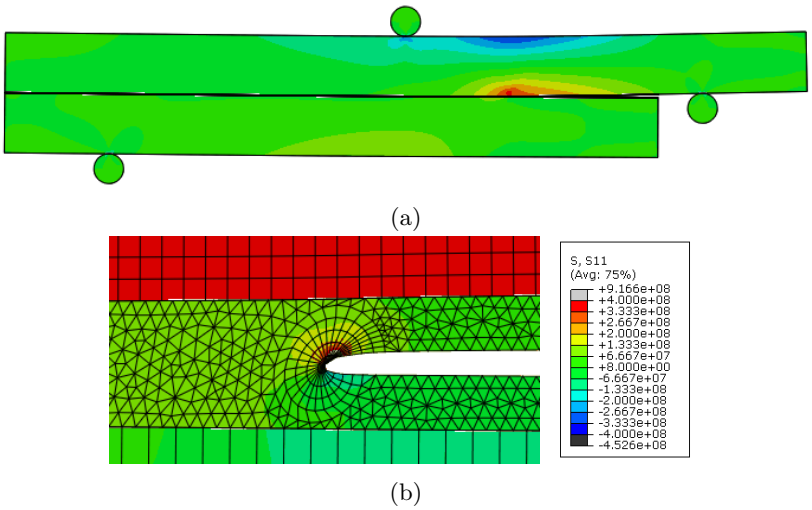

FIGURE 6: Longitudinal stress field in the SLB specimen : (a) General overview (b) zoom at the crack tip

mode fracture toughness determination using the SLB test can now be compared to the MMDCB test.

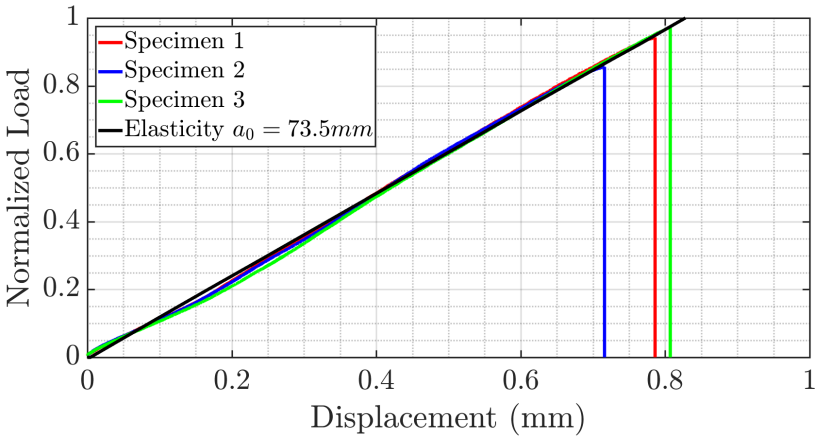

FIGURE 7: Load-displacement curves for a SLB specimen : comparison between simulation and experiments

3.3. MMDCB 45° testing

The specific preparation of the MMDCB specimens needs further information.

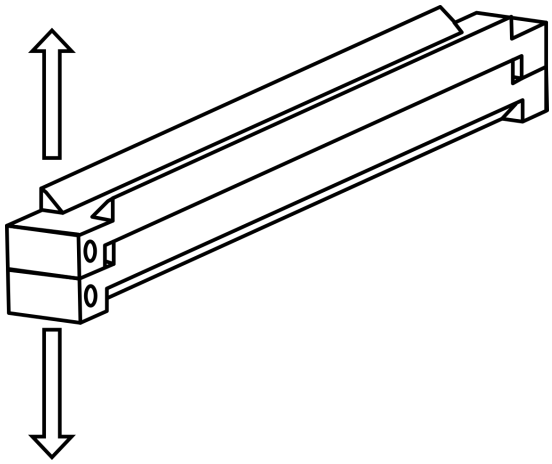

FIGURE 8: Perspective view of the MMDCB specimen

Flat heads and tails are observable on the schematic view of the MMDCB test in Figure 8. These flat parts were machined at each end of the MMDCB substrates. Thus, the thickness of the adhesive was directly calibrated with steel sheets, with a 200 μm thickness. The steel sheets were placed between each respective head and tail of the substrates. BIn addition, loading holes were created at the head of each substrate. The heads and tails were covered with a 3M silicone adhesive tape on a Teflon support. The tape was applied over 25 mm from the head so that the crack would initiate from its tip. In order to ensure that the silicone adhesive would not alter the epoxy curing, a transparent teflon film without any adhesive was used in the centre flat part of the MMDCB specimen. Thus, there was no bonding at the centre part of the MMDCB section, according to Figure 2b. The MMDCB specimens were then individually cured, with the curing procedure described in Section 3.1.
Quasi-static experiments were conducted using an electromechanical testing machine Instron 4302. The specimens were loaded under a constant crosshead speed up until the total failure of the sample. One test was conducted at a crosshead speed of 0.5 mm/min, and two others at 50 mm/min. The load was recorded with an Instron 2518-202 load cell. The load measurement range was fixed at 10kN. For all three tested specimens, the adhesive exhibited an unstable crack growth behaviour, similar to that observed during the SLB test. The fracture surfaces are shown in Figure 9. Synchronized marks on each side of the fracture surface suggest that the two cracks were always balanced. Thus, the assumption made in Section 2.2, about two balanced cracks in the MMDCB test, can be considered valid.

The MMDCB test is quite similar to the standard Mode I DCB test [18][25] . Thus, the extended Corrected Beam Theory with effective crack length (CBTE), whose accuracy was recently evaluated [24], can be adapted to the MMDCB test. The effective crack length can be calculated using the load P and the opening

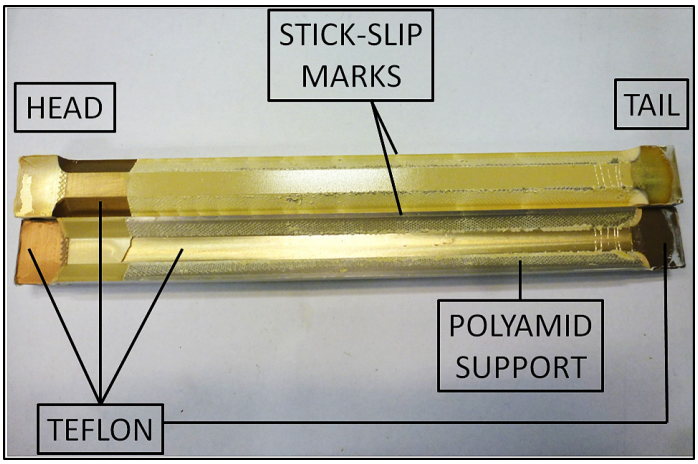

FIGURE 9: Rupture surfaces of a MMDCB specimen ($\alpha = 45°$, $\dot{\delta}$ =50mm/min)

displacement δ [26] as follows :

$$a = \left(\frac{3EI}{2} \frac{\delta}{P} \right)^{\frac{1}{3}} \tag{2}$$

where E is the Young modulus of the substrates and I the specific second moment of area of the MMDCB substrates. Consequently, the time history of the energy release rate can be obtained :

$$G = \left(\frac{9P^2\delta^2}{4EB^3I} \right)^{\frac{1}{3}} \tag{3}$$

where B is the crack front curvilinear length. Figure 10 shows the evolution of the energy release rate with respect to the crack length, using the CBTE analysis protocol.

The unstable behaviour can be observed with a visible drop from a peak value G_c, with a crack advance, up until an arrest energy release rate is reached. A new loading stage occurs and the operation is repeated. Considering only peak values, a mean value is obtained for each specimen, as detailed in Table 2. A mean value over the three specimens of $G_c/G_{Ic} = 2.02$ is found. Despite the need for more specimens to be tested, this value is clearly in agreement with the results obtained from the SLB test. Thus, the equivalence between the Mode II and the Mode III obtained in section 2.2 can be confirmed. The MMDCB test is found to be equivalent to the SLB test. In addition, contrary to the SLB test, a single MMDCB specimen allows multiple values of the fracture toughness to be determined.

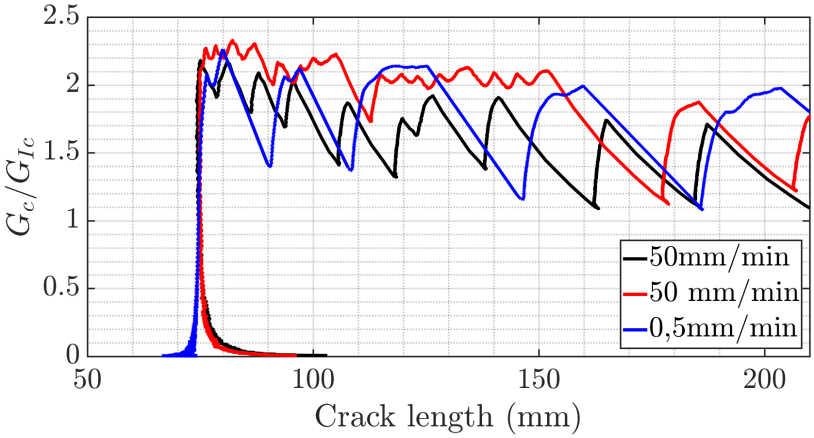

FIGURE 10: Experimental R-curves using the CBTE method

Specimen	$\dot{\delta}$ (mm/min)	$< G_c > /G_{Ic}$	$\sigma / < G_c >$ (%)
1	50	1.91	9.4
2	50	2.12	6.5
3	0.5	2.04	6.5

TABLE 2: Fracture toughness values and relative standard deviation for each MMDCB specimen tested

4. Numerical extension to dynamic loadings

The MMDCB test was designed for dynamic testing. Despite a specific substrate section, the MMDCB specimen is quite similar to the DCB one. Thus, the same drawbacks due to dynamic testing will be observed. Indeed, using a servohydraulic machine, the upper part of the specimen is loaded while the lower part is constrained vertically. Unsymmetric dynamic loading causes inertia effects such as unsymmetric flexure of the two substrates. The difficulty of performing symmetric dynamic DCB tests, in order to keep the desired mode mixity, has been addressed by several authors. A specific dual electromagnetic Hopkinson bar apparatus was recently adapted to perform symmetric DCB tests in the range of 10 to 30 m/s [27]. For intermediate loading rates, a complex apparatus developed by Hug et al. [28] allowed symmetric DCB tests to be performed up to 1.6 m/s.

The aim of this section is to numerically quantify the higher loading rate at which MMDCB tests can be performed without a specific apparatus, using a servohydraulic machine. Symmetric flexure is sought in this study for at least two reasons. The first one is the validity of the CBTE analysis. A symmetric flexure is required to model the specimen with two identical built-in beams. The second one is that the MMDCB mode mixity was calculated in Section 2.2, assuming a symmetric flexure in the two substrates. Therefore, it is necessary to

quantify the unsymmetric loading effects. A 3D explicit model of the MMDCB test was made. An overview of the mesh is shown in Figure 11.

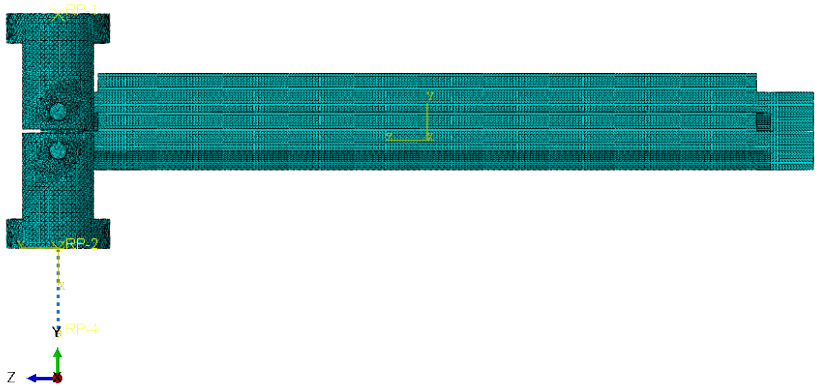

FIGURE 11: Overview of the finite element model

Two swivel pieces combined with pins are used to hold the MMDCB specimen. The two swivel pieces are meshed with tetrahedral elements C3D4, whereas hexahedral elements C3D8R were used for the two pins. All surface-to-surface contacts were modelled with a normal penalty contact interaction and with a shear friction coefficient taken as 0.05. The upper swivel is a piece made of steel (ρ=7.7 , E=210 GPa, ν=0.3) used to transmit the load from the servohydraulic jack to the MMDCB specimen. The surface at the top of the steel swivel is coupled to a reference point. This reference point is subjected to a vertical smooth step displacement amplitude δ in order to reproduce the dynamic loading. The same intermediate piece made of titanium (ρ=4.43, E=114 GPa, ν=0.34) is used to link the lower part of the MMDCB specimen to the lower holder, on which the load cell is mounted. This piece is made out of titanium, in order to maintain the fixture eigen frequency as high as possible. The load cell is located on this fixture. Thus, the filtering of the experimental load signal should be easier. In order to model the load signal measurement, a linear 1D spring was implemented with the respective stiffness and mass of a piezoelectric load cell Kistler 9031. The top of the spring is connected to the titanium swivel with a coupling constraint. The adhesive joint and the substrates were modelled as in Section 2.2.

4.1. Simulation under $\dot{\delta} = 10\ m/s$

An overview of the Von Mises field, for a test performed at $\dot{\delta} = 10\ m/s$, is shown in Figure 12, at $t = 1\ ms$. The unsymmetric flexure is observable

when comparing the stress fields of the two substrates. Antisymmetric stress concentrations are induced in the corners of the swivel pieces. The small difference between the stress fields in the two swivel pieces, is only due to their different material properties (steel and titanium). This unsymmetric flexure can be quantified with the measured load on each side of the model.

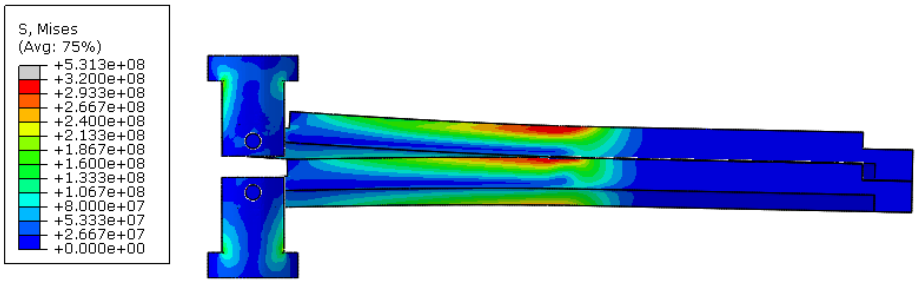

FIGURE 12

FIGURE 13: $\dot{\delta} = 10m/s$: Von Mises stress field in the 3D model at $t = 1\ ms$.

Indeed, using the loading reference point and the load cell, loads $P_{x/y}^{up/down}$ can be plotted in Figure 14. The subscript x/y refers to the horizontal and ver-

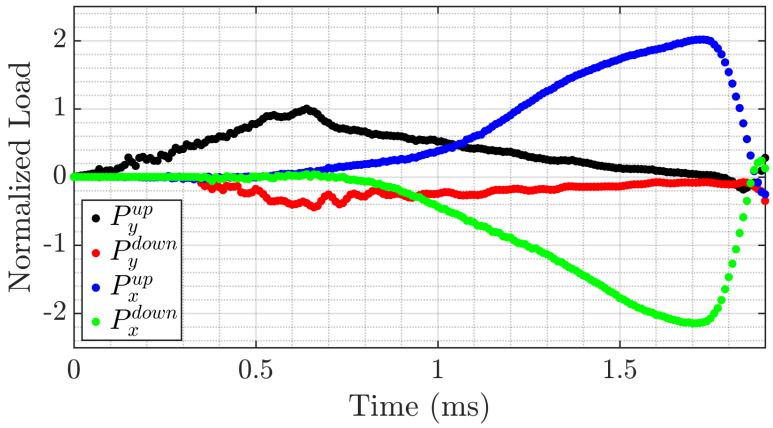

FIGURE 14: Normalized loads in the MMDCB simulation at the upper and lower reference points for $\dot{\delta} = 10$ m/s

tical loads, whereas the up/down superscript respectively refers to the upper and lower part of the 3D model. The load cell vibrational resonance is clearly observable in the P_y^{down} time history, where the peak load is difficult to identify. Thus, the experimental load cell signal should not be used in the CBTE analysis. Moreover, a horizontal load increases during the test, until sample failure occurs at approximately 1.75 ms. This horizontal load is consistent with the antisymmetric stress concentrations observed in the Von Mises field. Indeed, the inertia of the lower substrate delays its flexure, and buckling occurs. The flexure delay between the two substrates is progressively emphasized as the crack propagates. This explains why the horizontal load increases with time.
Finally, the mode mixity in the MMDCB specimen is highly altered. For a crack length $a = 180\ mm$, the standard deviation in the mode mixity along the crack front increased to 25 %. The mode mixity is no longer constant during the MMDCB test. Thus, any evaluation of the fracture toughness becomes questionable.

4.2. Simulation under $\dot{\delta} = 1\ m/s$

The same simulation was performed at a rate $\dot{\delta} = 1\ m/s$. For three successive crack lengths, the mode mixity along the crack front is plotted in Figure 15. The mean mode mixity slightly increased by 4.5 % for a crack length $a = 180\ mm$. G_s/G_t was then considered constant despite the unsymmetric loading.

The load time histories are plotted in Figure 16. The flexure delay due to inertia is reduced at a larger timescale, such that the horizontal load is lower than in Section 4.1. For a displacement rate of $\dot{\delta} = 1\ m/s$, oscillations are observed in the horizontal load. Indeed, the lower substrate progressively catches

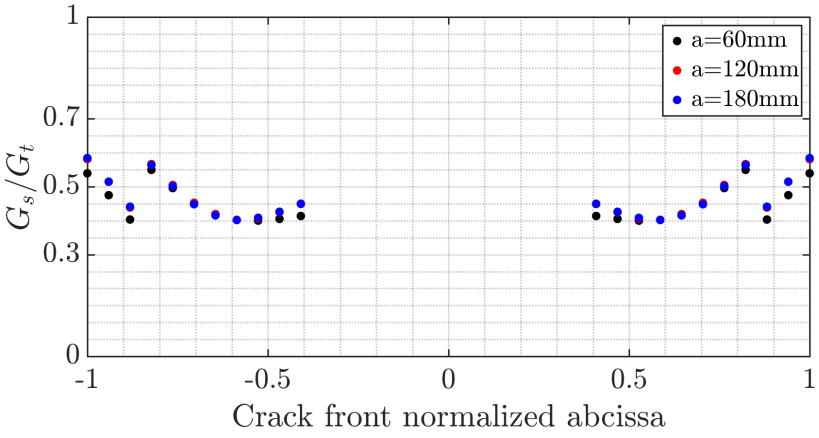

FIGURE 15: Mode mixity distribution for three successive crack lengths under $\dot{\delta} = 1\ m/s$

up its flexure delay, so the buckling diminishes. Then, the opposite phenomenom happens. These vibrations of the specimen tail are typical of the DCB test under intermediate dynamic loading rates [29]. Moreover, according to Figure 16, the load cell does not exhibit oscillations. The inlet in Figure 16 shows the good load balance on each side of the specimen. The vertical load time history of P_y^{down} is consistent with a static MMDCB test.

The energy release rate determination using the CBTE analysis can be performed. The vertical displacement from the loading reference point δ, and the vertical calculated load from the load cell P_y^{down} are used in Equation (3). The calculated energy release rate during the simulation is plotted in Figure 17.

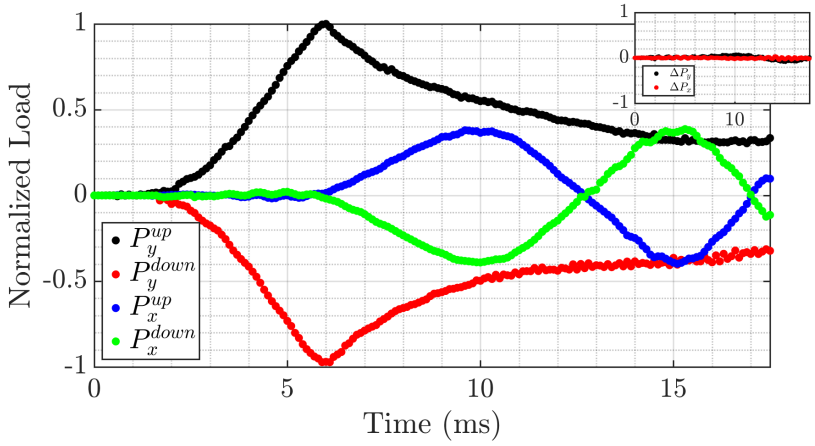

FIGURE 16: Normalized loads in the MMDCB simulation at the upper and lower reference points for $\dot{\delta} = 1\ m/s$

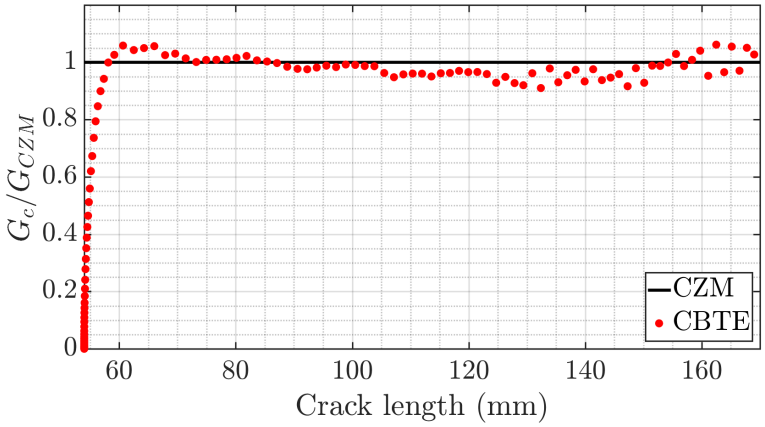

FIGURE 17: Comparison between the measured fracture toughness under $\dot{\delta}$ using the CBTE and the value from the CZM model

Its evolution with the crack length is compared to the fracture toughness value used by the authors in the cohesive zone model of the joint. The maximal relative error in the fracture toughness determination was 10% of the CZM value. Despite an unsymmetric flexure of the substrates, the CBTE analysis can be considered accurate up to a displacement rate of $\dot{\delta} = 1$ m/s. Thus, the unsymmetric loading can be neglected and the MMDCB test can be performed up to 1 m/s with a servohydraulic machine and an extended CBTE analysis protocol. However, a higher loading rate would emphasize the observed error in the fracture toughness determination. Beyond $\dot{\delta} = 1$ m/s, a symmetrical loading testing device should be used.

5. Conclusions

In this paper, a new specimen named MMDCB was developed to characterize the fracture behaviour of adhesives under mixed mode dynamic loading rates. A homogeneous mode mixity along the crack front, independent from the crack length, was achieved. The mode mixity was chosen, by considering a main angle α between the plane of the adhesive and the loading axis. MMDCB specimens with different angles α allow the full failure envelope to be explored from tensile to shear loading. Besides, contrary to the well known Mixed Mode Bending or the ARCAN test, the MMDCB test does not require a specific fixture. Nevertheless, its design relies upon the assumption that the fracture Mode II and III are equivalent. Consequently, for a given angle $\alpha = 45°$, experimental MMDCB quasi-static tests were compared to a reference SLB test, with the same mode mixity. The experiments were conducted on a viscoelastic viscoplastic epoxy adhesive with aluminum substrates. The SLB tests were analyzed using a J-integral analysis method. Each SLB specimen provided only one G_c

value, because of an unstable crack growth behaviour and a small useful bonding area. A single MMDCB specimen allowed multiple G_c evaluations thanks to a long useful bonding area. This test was analysed using the analytical corrected beam theory with effective crack length method (CBTE). The SLB and MMDCB tests showed good agreement. Indeed, the failure surfaces and the G_c evaluations were consistent. This good consistency confirmed the equivalence of failure Modes II and III for epoxy adhesives. The MMDCB test was then numerically validated under dynamic loadings up to 1m/s using explicit finite element simulations. Despite an unsymmetric loading, due to a servohydraulic testing machine, the MMDCB mode mixity was not significantly affected. The CBTE analysis protocol was also numerically proven to accurately measure the fracture toughness under a dynamic loading. In addition, beyond a loading rate of 1 m/s, the MMDCB test can still be performed with a symmetric loading fixture, such as a dual electromagnetic Hopkinson device.

Quasi-static and dynamic MMDCB tests with different angles should be performed. These tests would allow the full envelope to be explored from tensile to shear fracture, and with the rate-dependency.

6. Acknowledgements

The authors are particularly grateful to the French national research program PRC MECACOMP, and the French National Association of Technical Research ANRT, for funding this work.

7. Bibliography

[1] BRK Blackman, AJ Kinloch, FS Rodriguez Sanchez, WS Teo, and JG Williams. The fracture behaviour of structural adhesives under high rates of testing. *Engineering Fracture Mechanics*, 76(18) :2868–2889, 2009.

[2] Michael May, Olaf Hesebeck, Stephan Marzi, Wolfgang Böhme, Jörg Lienhard, Sebastian Kilchert, Markus Brede, and Stefan Hiermaier. Rate dependent behavior of crash-optimized adhesives–experimental characterization, model development, and simulation. *Engineering Fracture Mechanics*, 133 :112–137, 2015.

[3] Ludovic Dufour, Benjamin Bourel, Franck Lauro, Gregory Haugou, Nicolas Leconte, and Nicolas Carrere. Failure stress criterion for adhesively bonded joint at different strain rates by using dynamic arcan test device. In *EPJ Web of Conferences*, volume 94, page 01024. EDP Sciences, 2015.

[4] M Costa, R Carbas, M Benedita, E Marques, G Viana, LFM Da Silva, E Yokoi, S Nakada, and T Furusawa. Static assessment of the mixed-mode behaviour of three epoxy adhesives. *Engineering Fracture Mechanics*, 182 :552–565, 2017.

[5] Georgios Stamoulis, Nicolas Carrère, Jean-Yves Cognard, Peter Davies, and Claudiu Badulescu. On the experimental mixed-mode failure of adhesively bonded metallic joints. *International Journal of Adhesion and Adhesives*, 51 :148–158, 2014.

[6] Viswanathan Sundararaman and Barry D Davidson. An unsymmetric double cantilever beam test for interfacial fracture toughness determination. *International Journal of Solids and Structures*, 34(7) :799–817, 1997.

[7] T Kevin O'Brien. Mixed-mode strain-energy-release rate effects on edge delamination of composites. In *effects of defects in composite materials*. ASTM International, 1984.

[8] W Steven Johnson. Stress analysis of the cracked-lap-shear specimen : an ASTM round-robin. *Journal of testing and evaluation*, 15(6) :303–324, 1987.

[9] John H Crews Jr and James R Reeder. A mixed-mode bending apparatus for delamination testing. *NASA technical memorandum 100662*, 1988.

[10] Georgios Stamoulis and Nicolas Carrere. Investigating the influence of material non-linearity in the fracture properties of ductile adhesives submitted to mixed-mode loading. *Engineering Fracture Mechanics*, 179 :260–271, 2017.

[11] G Fernlund and JK Spelt. Mixed-mode fracture characterization of adhesive joints. *Composites Science and Technology*, 50(4) :441–449, 1994.

[12] David Joseph Pohlit. *Dynamic mixed-mode fracture of bonded composite joints for automotive crashworthiness*. PhD thesis, Virginia Tech, 2007.

[13] BRK Blackman, AJ Kinlock, FS Rodriguez-Sanchez, and WS Teo. The fracture behaviour of adhesively-bonded composite joints : Effects of rate of test and mode of loading. *International Journal of Solids and Structures*, 49(13) :1434–1452, 2012.

[14] Herzl Chai. Shear fracture. *International Journal of Fracture*, 37(2) :137–159, 1988.

[15] M Arcan, Z Hashin, and A Voloshin. A method to produce uniform plane-stress states with applications to fiber-reinforced materials. *Experimental mechanics*, 18(4) :141–146, 1978.

[16] Ludovic Dufour, Benjamin Bourel, Franck Lauro, Gregory Haugou, and Nicolas Leconte. A viscoelastic-viscoplastic model with non associative plasticity for the modelling of bonded joints at high strain rates. *International Journal of Adhesion and Adhesives*, 70 :304–314, 2016.

[17] Georgios Stamoulis, Nicolas Carrère, J-Y Cognard, Peter Davies, and Claudiu Badulescu. Investigating the fracture behavior of adhesively bonded metallic joints using the arcan fixture. *International Journal of Adhesion and Adhesives*, 66 :147–159, 2016.

[18] ASTM. D3433. *Standard Test Method for Fracture Strength in Cleavage of Adhesives in Bonded Metal Joints*, 2012.

[19] G.R.Irwin. Analysis of stresses and strain near the end of a crack traversing of a plate. *Journal of applied mechanics*, 1957.

[20] G.R.Irwin. Structural aspects of brittle fracture. *Applied materials research*, 1964.

[21] T Ungsuwarungsri and WG Knauss. The role of damage-softened material behaviour in the fracture of composites and adhesives. *International Journal of Fracture*, 35(3) :221–241, 1987.

[22] BD Davidson and V Sundararaman. A single leg bending test for interfacial fracture toughness determination. *International Journal of Fracture*, 78(2) :193–210, 1996.

[23] James R Rice. A path independent integral and the approximate analysis of strain concentration by notches and cracks. *Journal of Applied Mechanics*, 35 :379–386, 1968.

[24] Noëlig Dagorn, Gérald Portemont, Vincent Joudon, Benjamin Bourel, and Franck Lauro. Fracture rate dependency of an adhesive under dynamic loadings. *Accepted in Engineering Fracture Mechanics*. 10.1016/j.engfracmech.2020.107082.

[25] ISO 25217. Adhesives. *Determination of the mode I adhesive fracture energy of structural adhesive joints using double cantilever beam and tapered double beam specimens*, 2009.

[26] BRK Blackman and J Williams. Crack length determination difficulties in composites-their effect on toughness evaluation. International conference on fracture ICF, 2005.

[27] Huifang Liu, Xianghao Meng, Huawen Zhang, Hailiang Nie, Chao Zhang, and Yulong Li. The dynamic crack propagation behavior of mode I interlaminar crack in unidirectional carbon/epoxy composites. *Engineering Fracture Mechanics*, 215 :65–82, 2019.

[28] G Hug, P Thevenet, J Fitoussi, and D Baptiste. Effect of the loading rate on mode I interlaminar fracture toughness of laminated composites. *Engineering Fracture Mechanics*, 73(16) :2456–2462, 2006.

[29] BRK Blackman, JP Dear, AJ Kinloch, H Macgillivray, Y Wang, JG Williams, and P Yayla. The failure of fibre composites and adhesively bonded fibre composites under high rates of test. *Journal of Materials Science*, 30(23) :5885–5900, 1995.